

# Drive-Only Interaction Engineering via Dynamical Freezing

Songbo Xie,<sup>1</sup> Jiheng Duan,<sup>2,3</sup> and Sabre Kais<sup>1,\*</sup>

<sup>1</sup>*Department of Electrical and Computer Engineering,  
North Carolina State University, Raleigh, North Carolina 27606, USA*

<sup>2</sup>*Department of Physics and Astronomy, University of Rochester, Rochester, NY, 14627 USA*

<sup>3</sup>*University of Rochester Center for Coherence and Quantum Science, Rochester, NY, 14627 USA*

Freezing is usually used to suppress unwanted dynamics, but it can also be used to engineer interactions. We introduce freezing-induced interaction engineering, a drive-only control paradigm in which dynamically freezing an auxiliary subsystem reshapes the effective Hamiltonian of the remaining degrees of freedom. As a concrete realization, we consider a three-qubit architecture where a driven modulator  $M$  is coupled to one of two target qubits,  $Q_1$ , while  $Q_1$  and  $Q_2$  retain a fixed native exchange-type interaction. When  $M$  is frozen in a dressed eigenstate, its projection renormalizes the local Hamiltonian of  $Q_1$ . This makes the dressed-frame detuning between  $Q_1$  and  $Q_2$  controllable by the drive frequency. The native interaction can then be switched between two regimes: an interaction-off regime with large dressed-frame detuning, and an interaction-on regime with resonant exchange. In the interaction-on regime, the protocol realizes an iSWAP gate using the native  $Q_1Q_2$  coupling. Full lab-frame simulations show high-fidelity iSWAP dynamics and strong interaction suppression in the interaction-off regime. By combining native-coupling gate speed with drive-only operational simplicity, freezing-induced interaction engineering provides a route toward fast, drive-controlled entangling gates in fixed-frequency quantum architectures.

*Introduction.*—Freezing, broadly understood as dynamically constraining selected degrees of freedom, is usually associated with protection—once certain pathways are made inaccessible, unwanted evolution is suppressed and fragile quantum states can be protected [1]. This idea appears across quantum control, from the quantum Zeno effect [2–5] and bang-bang control [6–10] to spin-locking [11–13].

Much less explored is the possibility that freezing can be used not only to suppress dynamics, but also to engineer interactions. When part of a composite system is dynamically constrained, the interactions experienced by the remaining degrees of freedom are reshaped [14]. For example, if a subsystem  $Q_1$  is frozen in a state  $|\psi\rangle$  while interacting with another subsystem  $Q_2$  through  $V_{12}$ , the interaction is projected to  $\langle\psi|_1V_{12}|\psi\rangle_1$ , which acts only on  $Q_2$ . This projected operator modifies the effective Hamiltonian of  $Q_2$ , changing its subsequent dynamics [15]. Freezing therefore becomes not only a way to suppress dynamics, but also an active resource for Hamiltonian engineering.

This viewpoint is especially compelling for quantum computing, where interactions must be strong for fast entangling gates and dynamically switchable on and off. Existing approaches in many architectures follow two broad paradigms. Tuning-based schemes exploit strong native couplings by dynamically tuning qubit frequencies [16–18] or coupler-mediated interactions [19–21], enabling fast gates. Related state-controlled gates have also been proposed [22]. However, such tunability requires dynamically changing system parameters, which can introduce additional noise channels and calibration overhead. In contrast, drive-only control schemes avoid such tunability by generating interactions through driven processes [23, 24], but these drive-induced interactions are

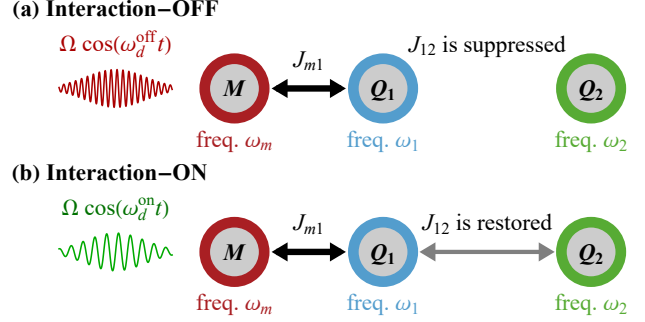


FIG. 1. Conceptual illustration of freezing-induced interaction engineering between two qubits  $Q_1$  and  $Q_2$  with transition frequencies  $\omega_1$  and  $\omega_2$ , coupled with strength  $J_{12}$ . An auxiliary modulator  $M$  with frequency  $\omega_m$  is coupled to  $Q_1$  with strength  $J_{m1}$ . Transverse drives applied to  $M$  realize two operating regimes: a drive at frequency  $\omega_d^{\text{off}}$  freezes  $M$  and suppresses the effective interaction between  $Q_1$  and  $Q_2$ , while a drive at  $\omega_d^{\text{on}}$  restores the interaction.

often higher-order processes and therefore weaker than direct native couplings [25]. This exposes a tension between the speed enabled by strong native interactions and the operational simplicity offered by drive-only control. Can one combine these two advantages in a single architecture?

The answer lies in freezing itself. In this work, we show that dynamical freezing can bridge the gap between native-interaction strength and drive-only control. We introduce a drive-only protocol in a generic three-qubit system, where an auxiliary modulator qubit controls a native interaction between two target qubits. The key mechanism is that freezing the modulator  $M$  in a dressed eigenstate renormalizes the local Hamiltonian of  $Q_1$ , allowing the  $Q_1Q_2$  interaction to be switched be-

tween detuned and resonant regimes without modifying the bare qubit frequencies during operation. This preserves the speed advantage of native coupling while enabling drive-only dynamical control. We also discuss a superconducting-circuit implementation, where the protocol can be realized using fixed-frequency transmons with microwave control.

*Freezing-induced interaction engineering.*—We aim to dynamically control the interaction between two primary qubits,  $Q_1$  and  $Q_2$ , without tuning their bare frequencies. We introduce an auxiliary modulator qubit  $M$  coupled to  $Q_1$ , while  $Q_1$  and  $Q_2$  retain a native exchange-type interaction. See Figure 1 for a conceptual illustration. Setting  $\hbar = 1$ , the three-qubit Hamiltonian with a transverse drive on  $M$  is

$$H_{m12} = -\frac{\omega_m}{2}\sigma_m^z - \frac{\omega_1}{2}\sigma_1^z - \frac{\omega_2}{2}\sigma_2^z + J_{m1}\sigma_m^x\sigma_1^x + J_{12}\sigma_1^x\sigma_2^x + \Omega\cos(\omega_d t)\sigma_m^x, \quad (1)$$

where  $\omega_m, \omega_1, \omega_2$  denote the qubit transition frequencies,  $J_{m1}, J_{12}$  are the native coupling strengths, and the last term represents a classical transverse drive applied to the modulator with amplitude  $\Omega$  and frequency  $\omega_d$ .

To reveal the freezing mechanism, we move to a rotating frame at the drive frequency  $\omega_d$ . Defining the detunings  $\Delta_i \equiv \omega_i - \omega_d$  for  $i \in \{m, 1, 2\}$  and applying the rotating-wave approximation (RWA), we obtain the rotating-frame Hamiltonian derived in Section I of the Supplemental Material (SM) [26]

$$H'_{m12} = H'_m - \frac{\Delta_1}{2}\sigma_1^z + \frac{J_{m1}}{2}(\sigma_m^x\sigma_1^x + \sigma_m^y\sigma_1^y) - \frac{\Delta_2}{2}\sigma_2^z + \frac{J_{12}}{2}(\sigma_1^x\sigma_2^x + \sigma_1^y\sigma_2^y), \quad (2)$$

where  $H'_m(\omega_d) \equiv \frac{\Omega}{2}\sigma_m^x - \frac{\Delta_m}{2}\sigma_m^z$  is the driven-modulator Hamiltonian with dressed splitting  $\omega'_m \equiv \sqrt{\Omega^2 + \Delta_m^2}$ . This describes a spin-locking configuration in which the modulator dynamics can be frozen in its dressed basis.

Specifically, the interaction between  $M$  and  $Q_1$  is effectively suppressed when their dressed-frame detuning  $\Delta'_{m1}$  is large compared to the coupling strength  $J_{m1}$ , described by the freezing condition

$$\Delta'_{m1} \equiv |\omega'_m - |\Delta_1|| \gg J_{m1}. \quad (3)$$

When this freezing condition is met, initializing  $M$  in an eigenstate of  $H'_m$  freezes its dynamics, allowing it to be treated as a static degree of freedom. Throughout this work,  $M$  is initialized and remains in its dressed ground state  $|g_m\rangle$  of  $H'_m(\omega_d)$ . Consequently, projecting the  $MQ_1$  interaction onto the modulator's frozen state reduces the three-qubit system to the effective two-qubit Hamiltonian

$$H'_{12}(\omega_d) = H'_1(\omega_d) + H'_2(\omega_d) + \frac{J_{12}}{2}(\sigma_1^x\sigma_2^x + \sigma_1^y\sigma_2^y). \quad (4)$$

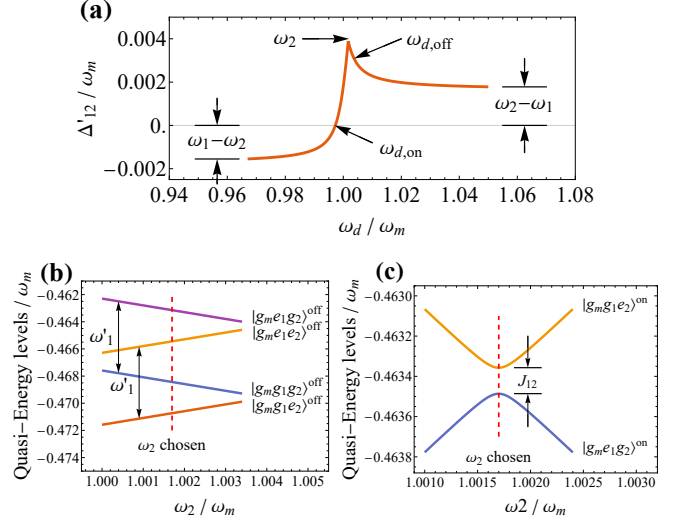


FIG. 2. (a) Effective detuning between qubits 1 and 2,  $\Delta'_{12}$ , as a function of the drive frequency  $\omega_d$ . In the limits  $\omega_d \rightarrow \pm\infty$ , the detuning approaches  $\Delta'_{12} \rightarrow \mp(\omega_1 - \omega_2)$ . The interaction-on regime corresponds to  $\omega_d = \omega_d^{\text{on}}$ , where  $\Delta'_{12} = 0$  and the qubits become resonant, while the interaction-off regime is chosen near  $\omega_d = \omega_d^{\text{off}}$ , where the detuning is near its maximum. (b) Floquet quasienergy spectrum in the interaction-off regime obtained by sweeping  $\omega_2$ . Only the four negative-energy branches, with the modulator fixed in  $|g_m\rangle$ , are shown. No avoided crossing occurs at the operating point, indicating large effective detuning and suppression of the  $Q_1Q_2$  interaction. (c) Floquet quasienergy spectrum in the interaction-on regime. At the operating point, an avoided crossing appears between the states  $|g_m g_1 e_2\rangle^{\text{on}}$  and  $|g_m e_1 g_2\rangle^{\text{on}}$ , signaling resonant energy exchange between  $Q_1$  and  $Q_2$  with a splitting set by  $J_{12}$ . Unless varied in the corresponding panel, the parameters are fixed at  $\omega_1 = 1$ ,  $\omega_2 = 1.0017$ ,  $J_{m1} = 0.0035$ ,  $J_{12} = 0.0001$ ,  $\Omega = 0.07$ , and  $\omega_d^{\text{off}} = 1.004$ , all in units of  $\omega_m$ . The red dashed lines in (b) and (c) indicate the chosen operating value of  $\omega_2$ .

Here  $H'_1(\omega_d) \equiv -\frac{\Delta_1}{2}\sigma_1^z + \frac{J_{m1}}{2}\langle\sigma_m^x\rangle\sigma_1^x + \frac{J_{m1}}{2}\langle\sigma_m^y\rangle\sigma_1^y$  is the effective local Hamiltonian of  $Q_1$  with dressed frequency  $\omega'_1 \equiv (\Delta_1^2 + J_{m1}^2\langle\sigma_m^x\rangle^2 + J_{m1}^2\langle\sigma_m^y\rangle^2)^{1/2}$ . Meanwhile,  $H'_2(\omega_d) = -\frac{\Delta_2}{2}\sigma_2^z$  is the local Hamiltonian of  $Q_2$  with dressed frequency  $\omega'_2 = |\Delta_2|$ . The expectation values  $\langle\sigma_m^x\rangle$  and  $\langle\sigma_m^y\rangle$  are taken in the frozen modulator state  $|g_m\rangle$ .

The freezing-renormalized detuning between  $Q_1$  and  $Q_2$ ,  $\Delta'_{12}(\omega_d) = |\omega'_1 - \omega'_2|$ , depends on the drive frequency  $\omega_d$  [see Fig. 2(a)]. This provides a direct handle for switching the effective  $Q_1Q_2$  interaction. We define the interaction-off and interaction-on regimes by the switching conditions

$$\Delta'_{12}(\omega_d^{\text{off}}) \gg J_{12} \quad \text{and} \quad \Delta'_{12}(\omega_d^{\text{on}}) = 0. \quad (5)$$

The first condition suppresses the native  $Q_1Q_2$  coupling through a large effective detuning, while the second restores it by bringing the two qubits into resonance.

We confirm these regimes through Floquet analysis [27, 28] by computing the single-period evolution operator  $U(\tau) = \mathcal{T} \exp[-i \int_0^\tau H(t) dt]$  with  $\tau = 2\pi/\omega_d$  and extracting the quasienergy spectrum from  $H_{\text{eff}} = \frac{i}{\tau} \log U(\tau)$ . As shown in Fig. 2(b), the interaction-off regime exhibits no avoided crossings between relevant energy levels, confirming effective suppression of the  $Q_1 Q_2$  coupling. In contrast, Fig. 2(c) shows a clear avoided crossing between  $|g_m g_1 e_2\rangle^{\text{on}}$  and  $|g_m e_1 g_2\rangle^{\text{on}}$  in the interaction-on regime, signaling resonant energy exchange while  $M$  remains frozen.

This avoided crossing provides the basis for gate operation. In a two-level exchange process with coupling strength  $J_{\text{eff}}$ , an iSWAP gate is realized after an evolution time  $T = \pi/(2J_{\text{eff}})$ . We realize this operation as follows. During idle operation, we set the drive frequency to  $\omega_d^{\text{off}}$  and prepare  $M$  in  $|g_m^{\text{off}}\rangle$ , thereby suppressing the effective  $Q_1 Q_2$  interaction. To implement an iSWAP gate, we switch to  $\omega_d^{\text{on}}$ , prepare  $M$  in  $|g_m^{\text{on}}\rangle$ , and hold the system for  $T_{\text{gate}} = \pi/(2J_{12,\text{eff}}^{\text{on}})$ , where  $J_{12,\text{eff}}^{\text{on}} = |\langle 0|g_1^{\text{on}}\rangle\langle 1|e_1^{\text{on}}\rangle|J_{12}$  is the effective coupling strength between  $Q_1$  and  $Q_2$  in the interaction-on regime, with  $|g_1^{\text{on}}\rangle$  and  $|e_1^{\text{on}}\rangle$  denoting the eigenstates of  $H_1'(\omega_d^{\text{on}})$  (see Section II of the SM [26]). This addresses the tension identified above: an iSWAP gate is generated by the native  $Q_1 Q_2$  coupling, while its on/off switching is controlled by the modulator drive.

*Quantifying on/off performance.*—We quantify the interaction-on performance by the average fidelity  $\overline{F}^{\text{on}}$ , obtained from ab initio simulations of the full lab-frame Hamiltonian in Eq. (1). For a given initial state of  $Q_1 Q_2$ , we evolve the full three-qubit system and apply the necessary local gates before and after the lab-frame evolution to compensate the rotating-frame phases and local dressed-qubit evolution. We then trace out the modulator  $M$ , obtaining an effective two-qubit channel in the interaction-on regime, denoted by  $\mathcal{E}^{\text{on}}$ . The fidelity is computed by comparing this output state with the state produced by the ideal iSWAP gate on the same input state. Since the ideal operation is unitary, the state fidelity is  $\langle \psi_{\text{ideal}} | \rho_{\text{out}} | \psi_{\text{ideal}} \rangle$ , where  $\rho_{\text{out}} = \mathcal{E}^{\text{on}}(|\psi_{\text{in}}\rangle\langle\psi_{\text{in}}|)$  and  $|\psi_{\text{ideal}}\rangle = U_{\text{iSWAP}}|\psi_{\text{in}}\rangle$ . The average fidelity  $\overline{F}^{\text{on}}$  is obtained by averaging this state fidelity over all possible initial states of  $Q_1 Q_2$ . The interaction-on performance is quantified by the infidelity  $\mathcal{I}^{\text{on}} \equiv 1 - \overline{F}^{\text{on}}$  (see Sections III and IV of the SM [26]).

To quantify the interaction-off performance, we use the detuning-to-coupling ratio

$$R_{\Delta/J}^{\text{off}} \equiv \Delta'_{12}(\omega_d^{\text{off}})/J_{12,\text{eff}}^{\text{off}}, \quad (6)$$

where  $J_{12,\text{eff}}^{\text{off}} = |\langle 0|g_1^{\text{off}}\rangle\langle 1|e_1^{\text{off}}\rangle|J_{12}$  is the effective  $Q_1 Q_2$  coupling strength in the interaction-off regime, with  $|g_1^{\text{off}}\rangle$  and  $|e_1^{\text{off}}\rangle$  denoting the eigenstates of  $H_1'(\omega_d^{\text{off}})$ . As shown below, this ratio consistently remains above 200 for the considered parameter settings, demonstrating strong suppression of the effective interaction in the interaction-off regime.

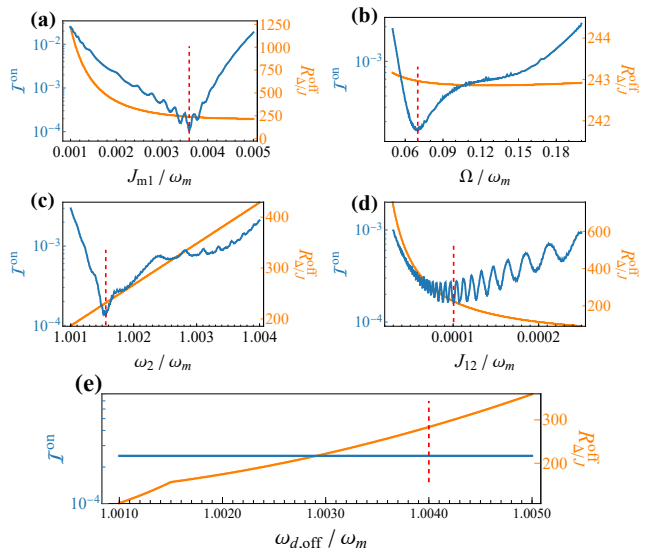


FIG. 3. Single-parameter scans of the protocol performance. Each panel varies one parameter while keeping the others fixed: (a)  $J_{m1}$ , (b)  $\Omega$ , (c)  $\omega_2$ , (d)  $J_{12}$ , and (e)  $\omega_d^{\text{off}}$ . The blue curves show the interaction-on infidelity  $\mathcal{I}^{\text{on}}$  obtained from full lab-frame simulations, while the orange curves show the interaction-off detuning-to-coupling ratio  $R_{\Delta/J}^{\text{off}}$ . Near the optimal points,  $R_{\Delta/J}^{\text{off}}$  remains larger than 200, indicating strong suppression of the effective  $J_{12}$ -mediated interaction in the interaction-off regime. Unless varied in the corresponding panel, the parameters are fixed at  $\omega_1 = 1$ ,  $\omega_2 = 1.0017$ ,  $J_{m1} = 0.0035$ ,  $J_{12} = 0.0001$ ,  $\Omega = 0.07$ , and  $\omega_d^{\text{off}} = 1.004$ , all in units of  $\omega_m$ . Red dashed lines indicate the optimal locations for the fixed-parameter setting.

*Parameter scans and optimization.*—The system contains eight control parameters, three of which can be fixed from simple physical considerations:  $\{\omega_m, \omega_1, \omega_d^{\text{on}}\}$ . The modulator frequency  $\omega_m$  sets the overall energy scale, and all other parameters are expressed in units of  $\omega_m$ . We set  $\omega_1 = \omega_m$  so that  $M$  and  $Q_1$  are resonant, maximizing the effect of the coupling  $J_{m1}$ . The on-regime drive frequency  $\omega_d^{\text{on}}$  is fixed by the switching condition  $\Delta'_{12}(\omega_d^{\text{on}}) = 0$ . The remaining five parameters are  $\{\omega_2, J_{m1}, J_{12}, \Omega, \omega_d^{\text{off}}\}$ .

These remaining parameters are constrained by the working conditions of the protocol. The freezing condition in Eq. (3) requires  $\Omega \gg J_{m1}$ , while the switching condition in Eq. (5) requires  $J_{m1} \gtrsim J_{12}$ . These conditions establish the hierarchy  $\Omega \gg J_{m1} \gtrsim J_{12}$ . Meanwhile,  $\Omega$  cannot be too large, since the RWA in Eq. (2) would otherwise break down. We therefore optimize these remaining parameters within this constrained parameter region by minimizing the interaction-on infidelity  $\mathcal{I}^{\text{on}}$ .

We first use single-parameter scans to illustrate the main parameter trends. In each scan, one of the five parameters  $\{J_{m1}, \Omega, \omega_2, J_{12}, \omega_d^{\text{off}}\}$  is varied while the others are fixed at  $J_{m1} = 0.0035$ ,  $J_{12} = 0.0001$ ,  $\Omega = 0.07$ ,  $\omega_2 = 1.0017$ , and  $\omega_d^{\text{off}} = 1.004$ , all in units of  $\omega_m$ . The re-

sulting average infidelities are shown in Figure 3. These scans illustrate local trends. A global optimum is obtained below by joint optimization.

Figure 3(a) shows the scan over  $J_{m1}$  and exhibits a minimum near  $J_{m1} \approx 0.0036\omega_m$ . This behavior reflects a balance between controllability and freezing. If  $J_{m1}$  is too small, the modulator has only a weak effect on  $Q_1$ , making the interaction switching inefficient. If  $J_{m1}$  is too large, the freezing condition Eq. (3) is weakened and the modulator no longer remains well confined to its initial dressed state.

Figure 3(b) shows the scan over  $\Omega$  and exhibits a minimum near  $\Omega \approx 0.07\omega_m$ . The lower side is limited by the freezing condition Eq. (3), since a weak drive cannot sufficiently freeze the modulator. The upper side is limited by the RWA used in Eq. (2), which becomes less accurate for excessively large drive amplitudes.

Figure 3(c) shows the scan over  $\omega_2$  and exhibits a minimum near  $\omega_2 \approx 1.0016\omega_m$ . If  $\omega_2$  is too close to  $\omega_1$ , the resonance condition in Eq. (5) can be satisfied only by choosing  $\omega_d^{\text{on}}$  far below the bare qubit frequencies. The resulting large rotating-frame detunings make the freezing condition in Eq. (3) harder to maintain, increasing the interaction-on infidelity. If  $\omega_2$  is too far from  $\omega_1$ , the available modulator-induced shift is insufficient to bring  $Q_1$  and  $Q_2$  into resonance in the interaction-on regime.

Figure 3(d) shows the scan over  $J_{12}$  and exhibits a minimum near  $J_{12} \approx 0.0001\omega_m$ . The nonmonotonic trend reflects a balance between signal strength and effective-model validity. For small  $J_{12}$ , the effective  $Q_1Q_2$  interaction is weak and is therefore more sensitive to any small residual detuning  $\Delta'_{12}$ , leading to a larger infidelity. This limitation arises with the current single-parameter scan and can be mitigated by optimizing remaining parameters jointly. For large  $J_{12}$ , Eq. (4) is no longer well reduced to a pure resonant exchange interaction. Since  $H'_1$  is aligned along a freezing-renormalized local axis, expressing the  $Q_1Q_2$  coupling in the local eigenbasis yields both the desired resonant exchange term and counter-rotating terms neglected under the eigenbasis RWA (see Section II of the SM [26]). As  $J_{12}$  increases, these neglected terms perturb the ideal iSWAP evolution.

Figure 3(e) shows that  $\mathcal{I}^{\text{on}}$  is independent of  $\omega_d^{\text{off}}$ . This is expected because  $\omega_d^{\text{off}}$  controls the interaction-off regime, while the plotted infidelity is for the interaction-on regime.

The orange curves in Fig. 3 show the corresponding detuning-to-coupling ratio  $R_{\Delta/J}^{\text{off}}$  in the interaction-off regime. For the parameter settings considered here, this ratio remains above 200 near the selected operating points, confirming strong suppression of the residual  $Q_1Q_2$  interaction when the coupling is switched off.

Guided by these trends, we next optimize the relevant parameters jointly. Since  $\omega_d^{\text{off}}$  does not affect the interaction-on infidelity, we fix it at  $\omega_d^{\text{off}} = 1.004\omega_m$  and optimize the remaining four parameters

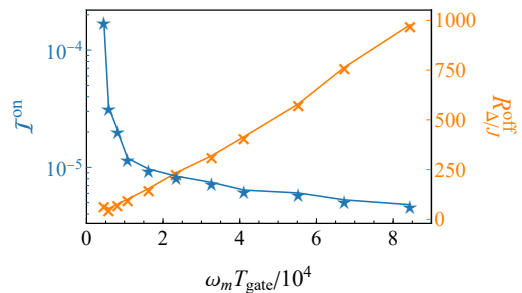


FIG. 4. Gate-time dependence of the interaction-on and interaction-off performance. The blue curve shows the optimized interaction-on infidelity  $\mathcal{I}^{\text{on}}$  as a function of gate time, and the orange curve shows the corresponding interaction-off detuning-to-coupling ratio  $R_{\Delta/J}^{\text{off}}$ . For each point,  $J_{12}$  and  $\omega_d^{\text{off}}$  are fixed, and  $\mathcal{I}^{\text{on}}$  is minimized over the remaining parameters  $\{J_{m1}, \Omega, \omega_2\}$ . The optimized  $\mathcal{I}^{\text{on}}$ , together with its corresponding  $R_{\Delta/J}^{\text{off}}$  and  $T_{\text{gate}}$ , is then extracted to form the plotted data point. The performance in both regimes improves with increasing gate time.

$\{J_{m1}, J_{12}, \Omega, \omega_2\}$ . This gives  $\mathcal{I}^{\text{on}} = 6.359 \times 10^{-6}$  at  $J_{m1} = 0.00216\omega_m$ ,  $J_{12} = 3.71 \times 10^{-5}\omega_m$ ,  $\Omega = 0.0876\omega_m$ , and  $\omega_2 = 1.000514\omega_m$ . This parameter set gives  $R_{\Delta/J}^{\text{off}} = 474.2$ . Together, this demonstrates high-fidelity iSWAP operation in the interaction-on regime and strong interaction suppression in the interaction-off regime. The time-domain dynamics for both regimes at this optimized operating point are shown in Section V of the SM [26].

We next examine the gate-time dependence of the optimized performance. For fixed values of  $J_{12}$  and  $\omega_d^{\text{off}}$ , we minimize  $\mathcal{I}^{\text{on}}$  over  $\{J_{m1}, \Omega, \omega_2\}$  and extract the corresponding  $\mathcal{I}^{\text{on}}$ ,  $R_{\Delta/J}^{\text{off}}$ , and  $T_{\text{gate}}$ . The resulting data are shown in Fig. 4. The interaction-on infidelity  $\mathcal{I}^{\text{on}}$  decreases as  $T_{\text{gate}}$  increases. This is expected because shorter gate times require larger  $J_{12}$ , making the switching condition in Eq. (5) harder to satisfy and thereby increasing the protocol infidelity. Meanwhile, the interaction-off detuning-to-coupling ratio  $R_{\Delta/J}^{\text{off}}$  increases almost linearly with  $T_{\text{gate}}$ . This follows from  $T_{\text{gate}} \propto 1/J_{12, \text{eff}}^{\text{on}}$  and  $R_{\Delta/J}^{\text{off}} \propto 1/J_{12, \text{eff}}^{\text{off}}$ , with both effective couplings originating from the same native coupling  $J_{12}$ . Consequently, increasing the gate time simultaneously improves the interaction-on fidelity and the interaction-off suppression.

*Superconducting-circuit implementation.*—The protocol is naturally suited to superconducting transmon circuits, which support pairwise exchange-type coupling and local microwave driving [29, 30]. A minimal implementation uses three fixed-frequency transmons: an auxiliary modulator  $M$  coupled to  $Q_1$ , and  $Q_1$  coupled to  $Q_2$ . A transverse microwave drive applied to  $M$  switches the system between the interaction-off and interaction-on regimes.

The optimized protocol requires the device parameters to lie in the appropriate range. While exact val-

ues may be difficult to achieve by fabrication alone, static tuning elements can be used during calibration to fine-tune the parameters. These adjustments are performed only once and remain fixed during gate operation. The entangling gate therefore requires neither dynamical qubit-frequency tuning nor tunable couplers; the only time-dependent control is the microwave drive on  $M$ . A circuit-level derivation of the transmon Hamiltonian and order-of-magnitude parameter-feasibility estimates are provided in Section VI of the SM [26].

*Summary.*—We have shown that dynamical freezing can serve as an active resource for interaction engineering. In a three-qubit architecture, freezing an auxiliary driven modulator reshapes the dressed-frame Hamiltonian of a target qubit, allowing a fixed native  $Q_1Q_2$  interaction to be switched between interaction-off and interaction-on regimes. The off regime arises from a large dressed-frame detuning, whereas the on regime restores resonant exchange and implements an iSWAP gate through the native  $Q_1Q_2$  coupling. Ab initio lab-frame simulations demonstrate high-fidelity interaction-on dynamics together with strong interaction-off suppression. More broadly, these results identify dynamical freezing as a general tool for Hamiltonian engineering, in which a frozen auxiliary degree of freedom is used to program effective interactions. By combining native-coupling gate speed with drive-only operational simplicity, freezing-induced interaction engineering provides a route toward fast, drive-controlled entangling gates in fixed-frequency quantum architectures.

*Acknowledgment.*—We thank Dr. Zihao Wang for valuable suggestions and Dr. Feiyang Ye for helpful discussions. We acknowledge support from the US Department of Energy, Office of Basic Energy Sciences, through the Quantum Photonic Integrated Design Center (QuPIDC) EFRC award DE-SC0025620.

---

\* skais@ncsu.edu

- [1] P. Facchi and S. Pascazio, *J. Phys. A: Math. Theor.* **41**, 493001 (2008).
- [2] B. Misra and E. G. Sudarshan, *J. Math. Phys.* **18**, 756 (1977).
- [3] W. M. Itano, D. J. Heinzen, J. J. Bollinger, and D. J. Wineland, *Phys. Rev. A* **41**, 2295 (1990).
- [4] F. Schäfer, I. Herrera, S. Cherukattil, C. Lovecchio, F. S. Cataliotti, F. Caruso, and A. Smerzi, *Nature communications* **5**, 3194 (2014).
- [5] R. Liu, X. Yang, X. Lv, X. Long, H. Liu, D. Lu, Y. Dong, and J. Li, *Phys. Rev. Lett.* **135**, 250805 (2025).
- [6] L. Viola and S. Lloyd, *Physical Review A* **58**, 2733 (1998).
- [7] L. Viola, S. Lloyd, and E. Knill, *Phys. Rev. Lett.* **83**, 4888 (1999).
- [8] J. J. Morton, A. M. Tyryshkin, A. Ardavan, S. C. Benjamin, K. Porfyakis, S. A. Lyon, and G. A. D. Briggs, *Nature Physics* **2**, 40 (2006).
- [9] G. S. Uhrig, *Phys. Rev. Lett.* **98**, 100504 (2007).
- [10] S. Damodarakurup, M. Lucamarini, G. Di Giuseppe, D. Vitali, and P. Tombesi, *Phys. Rev. Lett.* **103**, 040502 (2009).
- [11] N. Timoney, I. Baumgart, M. Johanning, A. Varón, M. B. Plenio, A. Retzker, and C. Wunderlich, *Nature* **476**, 185 (2011).
- [12] J. H. Bodey, R. Stockill, E. V. Denning, D. A. Gangloff, G. Éthier-Majcher, D. M. Jackson, E. Clarke, M. Hugues, C. L. Gall, and M. Atatüre, *npj Quantum Information* **5**, 95 (2019).
- [13] I. Zuk, D. Cohen, A. V. Gorshkov, and A. Retzker, *Physical Review Research* **6**, 013217 (2024).
- [14] S. Xie, M. Sajjan, and S. Kais, *Entropy* **27**, 1147 (2025).
- [15] S. Xie, M. Sajjan, A. Ajoy, and S. Kais, arXiv:2506.18276 (2025).
- [16] F. W. Strauch, P. R. Johnson, A. J. Dragt, C. Lobb, J. Anderson, and F. Wellstood, *Phys. Rev. Lett.* **91**, 167005 (2003).
- [17] A. Dewes, F. R. Ong, V. Schmitt, R. Lauro, N. Boulant, P. Bertet, D. Vion, and D. Esteve, *Phys. Rev. Lett.* **108**, 057002 (2012).
- [18] R. Barends, J. Kelly, A. Megrant, A. Veitia, D. Sank, E. Jeffrey, T. C. White, J. Mutus, A. G. Fowler, B. Campbell, *et al.*, *Nature* **508**, 500 (2014).
- [19] A. Blais, A. M. van den Brink, and A. M. Zagoskin, *Phys. Rev. Lett.* **90**, 127901 (2003).
- [20] R. Bialczak, M. Ansmann, M. Hofheinz, M. Lenander, E. Lucero, M. Neeley, A. O’Connell, D. Sank, H. Wang, M. Weides, *et al.*, *Phys. Rev. Lett.* **106**, 060501 (2011).
- [21] Y. Chen, C. Neill, P. Roushan, N. Leung, M. Fang, R. Barends, J. Kelly, B. Campbell, Z. Chen, B. Chiaro, *et al.*, *Phys. Rev. Lett.* **113**, 220502 (2014).
- [22] S. E. Rasmussen and N. T. Zinner, *Phys. Rev. Research* **2**, 033097 (2020).
- [23] J. M. Chow, A. D. Córcoles, J. M. Gambetta, C. Rigetti, B. R. Johnson, J. A. Smolin, J. R. Rozen, G. A. Keefe, M. B. Rothwell, M. B. Ketchen, *et al.*, *Phys. Rev. Lett.* **107**, 080502 (2011).
- [24] J. M. Chow, J. M. Gambetta, A. W. Cross, S. T. Merkel, C. Rigetti, and M. Steffen, *New J. Phys.* **15**, 115012 (2013).
- [25] E. Magesan and J. M. Gambetta, *Phys. Rev. A* **101**, 052308 (2020).
- [26] Supplemental material (2026).
- [27] J. H. Shirley, *Phys. Rev.* **138**, B979 (1965).
- [28] H. Sambe, *Phys. Rev. A* **7**, 2203 (1973).
- [29] J. Koch, T. M. Yu, J. Gambetta, A. A. Houck, D. I. Schuster, J. Majer, A. Blais, M. H. Devoret, S. M. Girvin, and R. J. Schoelkopf, *Phys. Rev. A* **76**, 042319 (2007).
- [30] A. Blais, A. L. Grimsmo, S. M. Girvin, and A. Wallraff, *Reviews of Modern Physics* **93**, 025005 (2021).